Journal of Volcanology and Geothermal Research, 53 (1992) 103–116
Elsevier Science Publishers B.V., Amsterdam

The magma system of Mount St. Helens: non-linear high-resolution P-wave tomography

Jonathan M. Lees

Yale University, Department of Geology and Geophysics, P.O. Box 6666, 210 Whitney Avenue, New Haven, CT 06511-8130, USA

(Received January 20, 1992; revised and accepted April 15, 1992)

ABSTRACT

Lees, J.M., 1992. The magma system of Mount St. Helens: non-linear high-resolution P-wave tomography. *J. Volcanol. Geotherm. Res.*, 53: 103–116.

High-resolution, three-dimensional images of P-wave velocity anomalies below Mt. St. Helens, Washington, were derived using tomographic inversion. The model is a $27.5 \times 21 \times 20$ km target volume parameterized by blocks 0.5 km per side. The area included 39 stations and 5454 local events leading to 35,475 rays used in the inversion. To diminish the effects of noisy data, the Laplacian was constrained to be small within horizontal layers, providing smoothing of the model. Non-linear effects were compensated for by iterating three-dimensional ray tracing (using pseudo-bending) between inversions and relocating earthquakes relative to the updated three-dimensional model. The structural differences between the linear and non-linear inversions appear to be insignificant, although the amplitudes of the anomalies are larger in the non-linear models. Results indicate a low-velocity anomaly (> 7%), approximately 1 km in lateral extent, from 1.5 to 3 km depths. Between 3 and 6 km depth the anomaly appears to spread out. Below 6 km depth the low-velocity feature changes to a higher-velocity perturbation with lower-velocity perturbations flanking around the perimeter of the volcano. The higher-velocity material, which correlates with the higher seismicity at that depth, is interpreted as being a plug capping the low-velocity magma chamber which begins below 9 km depth.

Introduction

Seismic imaging of structures below volcanoes has become a standard tool for clarifying the extent of magmatic bodies in areas where dense seismic arrays allow us to apply the methods of computed tomography. Local earthquake data were used to illuminate features below Kilauea (Thurber, 1984), Mt. St. Helens (Lees and Crosson, 1989), Campi Flegrei, Italy (Aster and Meyer, 1988), and Long Valley Caldera (Kissling, 1988). Teleseismic seismic arrivals have also been used to determine the extent of magmatic bodies below quaternary volcanoes (Achauer et al., 1988; Iyer et al., 1990) and active seismic sources have also been used at Newberry volcano (Evans and Zucca, 1988). In all of these studies anomalously low-velocity zones were interpreted as imaging magma reservoirs at depth. In general the spatial resolution of these previous analyses has been about 5–10 km at best and often worse.

Geophysical investigations of the subsurface structure of the Mt. St. Helens edifice include primarily gravity modeling (Williams et al., 1987), aeromagnetic modeling (Finn and Williams, 1987), studies of the seismicity (Weaver and Smith, 1983; Fehler, 1985; Scandone and Malone, 1985; Shemeta and Weaver,

Correspondence to: J.M. Lees, Yale University, Department of Geology and Geophysics, P.O. Box 6666, 210 Whitney Avenue, New Haven, CT 06511-8130, USA.

1986; Weaver et al., 1987; Endo et al., 1990) and geochemical methods (Rutherford et al., 1985; Rutherford and Devine, 1988). The commonly accepted model for the magma system below Mt. St. Helens (Scandone and Malone, 1985) proposes the existence of a magma body at 7–9 km depth with 10–20 km^3 volume. A conduit, with a radius of approximately 50 m, was suggested to feed the crater at the surface with no evidence of a shallow magma chamber. This model was later confirmed by seismicity studies; however, a small aseismic zone between 2 and 3 km depth indicated the possible presence of a shallow magma reservoir (Shemeta and Weaver, 1986). A localized, layered velocity model for the detailed study of earthquake locations further confirmed the suggestion that the aseismic zone indicated the presence of a magma reservoir at 3–4.5 km depth (Endo et al., 1990). Earthquake focal mechanisms have also been used to model a 5–7 km^3 magma body between 7 and 11 km depth (Barker and Malone, 1991). Modeling of the stress field supported the conclusion that the magma body was 0.6 km north of the present dome and cylindrically shaped with a radius of 0.75 km.

In this study I have used an extensive set of local earthquake data to derive a detailed model of the subsurface structure of Mt. St. Helens which resolves features on the order of 1 km or less. This is probably an upper limit on the spatial resolving power of this data set due to the bandwidth limitations of the seismic instrumentation and recording system. The model differs significantly from previous models of Mt. St. Helens in that a major low-velocity anomaly is observed in the shallow region and a high-velocity anomaly is seen between 6 and 9 km depth in contrast to earlier magma images that were found to start at 7 km depth (Lees and Crosson, 1989).

Data selection and reference model

The arrival times used in this study were selected from the earthquake catalogue of the University of Washington. The bounding target area spanned 27.5 km east–west (122°1.67′–122°23′) and 21 km in the north–south direction from 46°5′ to 46°17.7′ and earthquakes were chosen ranging in date from 1980 to 1990 (Fig. 1). Among the 10,942 earthquakes in the catalogue 5454 were deemed of high enough quality factor (root mean square travel time residual <0.3 s, horizontal error <2.5 km, vertical error <5.0 km, seismic gap $<135°$ and minimum distance $<$ maximum of either twice the hypocentral depth or 5 km) to be used. After relocation and determination of station corrections by iteratively adjusting event locations and station delays until residual distributions for each station appeared to have approximately zero mean, 5156 events remaining in the target volume provided 35,475 raypaths for use in the inversion. It may seem reasonable to divide the data according to observed changes in seismicity, or other observable phenomena, to attempt to monitor changes in the magma structures over time. My few attempts at this, however, did not provide any discernible differences during this time period.

The initial one-dimensional model was derived using the method of progressive multiple event location (Malone and Pavlis, 1983; Pavlis and Booker, 1983). This layered model, called SH3, is the standard one-dimensional model used for routine earthquake locations in the Mt. St. Helens region, which spans approximately an 80 km square centered on the volcano. An alternative one-dimensional model derived by Endo et al. (1990) differs from the SH3 model primarily in the top 3 km where the velocities were considerably slower than the SH3 model. This model, however, would be appropriate only for events and stations that are very near the volcano itself, as the data used in its determination were entirely local. As will be seen below, the three-dimensional model derived in this study, which is a perturbation of the SH3 model, also exhibits a shallow low-velocity zone relative to the SH3 model, but as

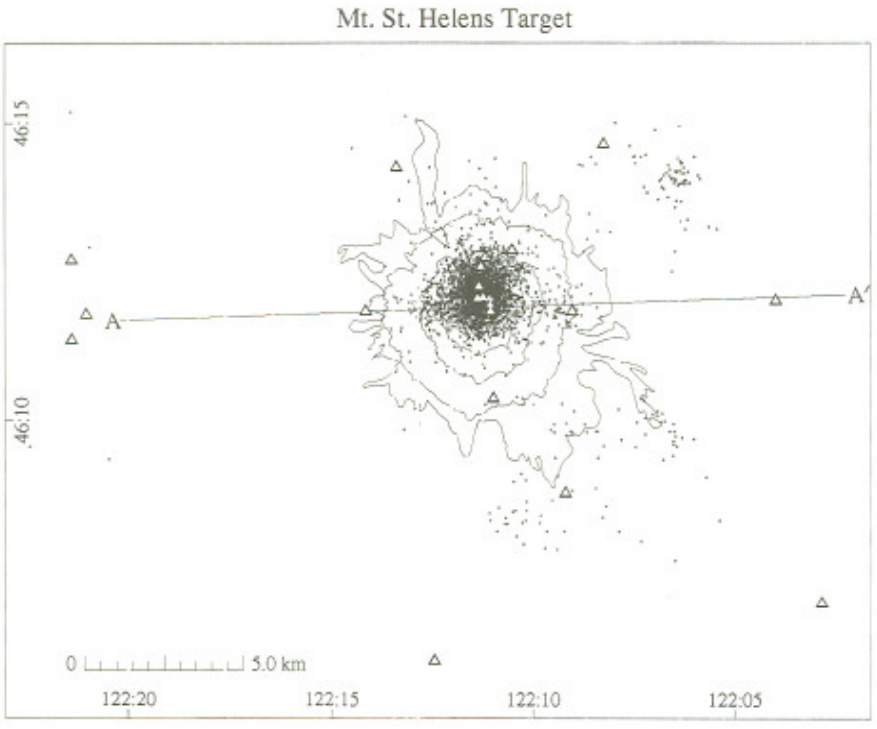

Fig. 1. Plan view of the Mount St. Helens target area. The 1000 m contours are plotted for reference where the outermost contour is the tree line prior to the 1980 eruption. Triangles are locations of seismic recording stations and small circles are epicenters of the data used in this study. Cross-section A–A' is shown in Figure 4.

a three-dimensional model it localizes the perturbation to a narrow zone below the crater.

Methodology

The target volume was divided into a 55×42 grid region using 0.5 km-square blocks of varying thickness following the 1-dimensional reference velocity models, resulting in a maximum of 24,000 model parameters. Rays were initially traced through the 1-dimensional models and perturbations of slowness were calculated within each block of the three-dimensional model such that the sum of the squared travel time residuals (observed minus predicted) is minimized. This initial step represents a first-order linear adjustment (Aki et al., 1977; Humphreys and Clayton, 1988) which reduced the weighted root mean square misfit by 20%. The data in the inversion were weighted according to estimates of the reading error (δt in seconds) determined by the seismic analyst who recorded the original arrival time measurement. (These same weights are used in the hypocenter location phase of the non-linear analysis.) In addition, the potentially biasing effects of large clusters of rays were removed by down-weighting heavily traveled paths inversely according to the number of rays along such paths. Ray clusters were determined by counting the number of rays from each block to each station. The ray clusters that had counts greater than 10 were down-weighted.

Non-linear inversions—hypocentral relocation and smoothing

Non-linear inversion is achieved by iterating over linear inversions after raypaths and

earthquake hypocenters are updated to include the most current three-dimensional model available. Perturbations from the current model are computed by applying linear inversion at each successive step as described above. The iterative process should converge to the non-linear result where the model does not change significantly. Inversions using earthquake data are especially non-linear because earthquake hypocenters are also functions of the current model.

Effects of noise in the data can result in models that have very high variance. To damp out these effects the two-dimensional Laplacian of the model in horizontal layers is required to be small while in the vertical direction there are no additional constraints (Lees and Crosson, 1989). This approach is taken, in part, because the dimensions of the model are small in the vertical dimension as compared to the horizontal, so models tend to be over-smoothed vertically if we use the same smoothing parameters in both dimensions. We may, of course, impose different smoothing constraints for the vertical dimension. In this study I have avoided this additional complication by choosing no smoothing for the vertical direction. For the linear analysis the matrix equation that must then be inverted is:

$$\begin{bmatrix} \mathbf{WA} \\ \lambda \mathbf{L} \end{bmatrix} \delta \mathbf{s} = \begin{bmatrix} \mathbf{W}t \\ \mathbf{0} \end{bmatrix} \qquad (1)$$

where δs is a vector of slowness perturbations, t is a vector of travel time residuals, $\mathbf{A}$ is the matrix describing the raypaths (the partial derivative of time with respect to slowness parameters), $\mathbf{W}$ is the (diagonal) covariance matrix of the data, $\mathbf{L}$ is the two-dimensional Laplacian and λ is the damping parameter (Lees and Crosson, 1989). When proceeding to the non-linear inversions, we search for perturbations from the previous (most current) inversion result. To insure that the full slowness models we derive have small Laplacian (and not just the most recent perturbations) equation (1) is modified by adding a non-zero part to the lower right-hand side:

$$\begin{bmatrix} \mathbf{WA} \\ \lambda \mathbf{L} \end{bmatrix} \delta s = \begin{bmatrix} \mathbf{W}t \\ -\lambda \mathbf{L} s_0 \end{bmatrix} \qquad (2)$$

where s_0 represents the previous model derived (Shaw and Orcutt, 1985; VanDecar, 1991). This leads to minimization of the following desired functional:

$$\min\{\|\mathbf{WA}\delta s - \mathbf{W}t\|^2 + \lambda^2 \|\mathbf{L}(\delta s + s_0)\|^2\} \qquad (3)$$

As there is currently no good *a priori* method for determining the best smoothing, the damping parameter, λ, is chosen, at least for now, by trial and error. A word of caution is in order. As the non-linear inversions explain more and more of the data residual, eventually the noise level of the data is reached, although we currently do not know where that level is precisely. (While we have a fairly good estimate for the variance of individual arrival-time picks, there are other sources of error that are not well constrained, such as parameterization error and hypocenter mislocation error.) The smoothing, or other, *a priori* constraints we place on the data may change. For example, for the non-linear inversions the damping parameter may be increased (more damping) with successive iterations as the residuals get smaller and approach the noise level. In this study the damping parameter was fixed for all iterations. The final overall data misfit was 47% less than the misfit associated with the starting reference model. The differences between the first-order linear inversions and the non-linear analysis in this study are not significant, at least in so far as the interpretation of the structural features is concerned. The two models differ primarily in the amplitude of the anomalies observed. As the amplitudes are heavily influenced by the smoothing, or damping, imposed on the inversion, and this a priori constraint is chosen rather arbitrarily, I am reluctant to assign particular significance to the absolute magnitude of velocities derived here. Rather, I am more confident in the relative perturba-

tions and how they are distributed spatially in the model. The geologic interpretations are thus a combination of the structural features observed here and assumptions regarding the nature of volcanoes in general (e.g. that somewhere at depth there exists a body of anomalously hot, perhaps molten, material.)

Ray-tracing

Ray-tracing in three-dimensional media is achieved through the pseudo-ray-bending method of Um and Thurber (1987). For the block parameterization used in this study I have had to make an approximation because the gradient of the slowness field is zero inside a block of constant slowness. To accommodate this difficulty a linear interpolation of slownesses using the centers of each block as nodes, was used for calculating gradients along raypaths. The actual predicted travel times, however, were calculated using the block velocities as in the original inversion program. This was necessary because a small additional travel time is nearly always added when the averaged slownesses are used for integrating along the raypath. This small extra time will bias the travel time residuals enough to cause artifacts in the final result. The linear interpolation scheme was therefore only used in calculation of the bending of raypaths.

A major difficulty with the ray-bending technique is the possibility that the raypath may converge to a local minimum travel time rather than the actual global minimum travel time path. This is because this method relies on an initial path from which small perturbations are calculated based on the local gradient of the slowness field. I have found examples of raypaths which remained in local minima both for initial paths that included only two starting nodes (source and receiver points in the model) and those starting with many nodes along one-dimensional model raypaths. The ray-bending method therefore does not provide any inherent guarantee that the final path is the shortest. For the block inversions, I found that a reliable scheme was to use two starting nodes when the raypath was determined to be a direct path, relative to the one-dimensional model and a path of 17 equally spaced, points along the sampled, one-dimensional refraction raypath. This requirement insured that refractions as determined by the one-dimensional model predominantly remained so in the three-dimensional model because the final raypaths were only slightly perturbed from the initial raypaths. For the inversions derived in this study, where the slowness perturbations and their gradients are relatively small, this is not an unreasonable approach, as we would expect the three-dimensional raypaths to be fairly close to the starting raypaths. The maximum number of nodes allowed in the raypath determination was 64. We are currently examining alternative raypath determination techniques which do guarantee the global minimum travel time path (Moser, 1991).

Event relocation is achieved by application of a damped least squares inversion for perturbations of earthquake hypocentral parameters (Geiger's method). By separating the slowness inversion and the hypocenter re-location I have assumed at each stage that the model/hypocenters used are exactly correct, at least until the next update when they are modified. This assumption entails a bias in the results for which I do not have an estimate. An alternative to this approach, which decouples the separate problems of hypocenter determination and velocity inversion by matrix projection (Pavlis and Booker, 1980; Thurber, 1983) was not attempted because of prohibitive computer storage and time required for such a large data set and model space. I note here, though, that these alternative, unbiased methods involve other assumptions which may be equally objectionable, such as hypocenter locations lying outside the earth, but this issue is beyond the scope of the present paper. The earthquake relocation program is thus simply the one-dimensional location program modified to cal-

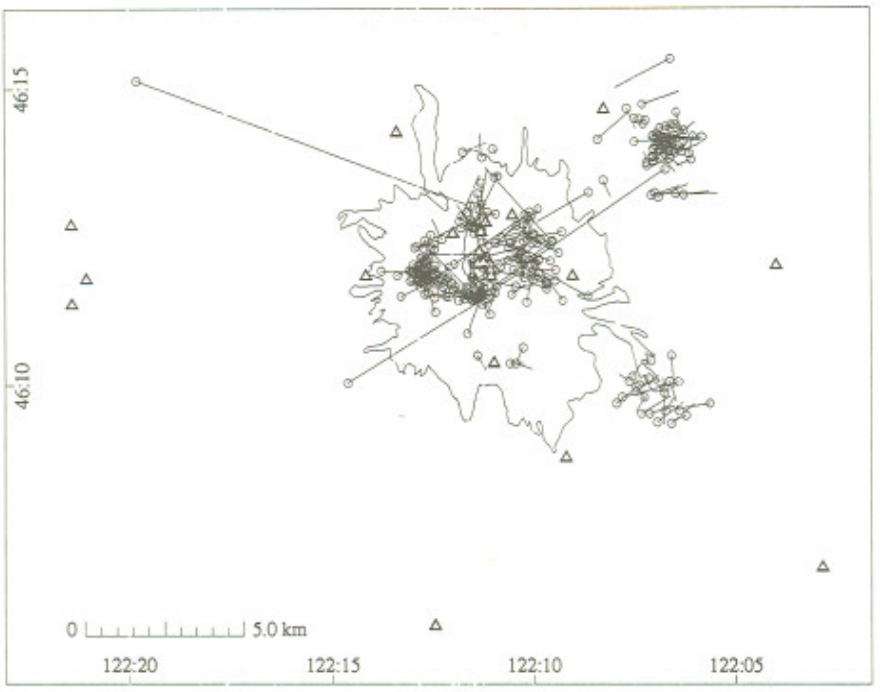

Fig. 2. A selection of earthquake epicenters plotted before and after relocation with the three-dimensional model. Circles represent the final location relative to the three-dimensional model and the lines point to the original locations relative to the SH3 model.

culate travel times relative to the three-dimensional model as described above. Only P-wave arrival times are used in this scheme as no three-dimensional S-wave model was derived. (Only P-wave arrival times were used as S-wave arrival time measurements from vertical sensors are widely known to be subject to large errors.) All 5454 of the earthquakes were relocated between each iteration and earthquakes which did not fit the original selection criteria were excluded. Generally the mislocations were small, about 0.5 km or less, although some of the events experienced hypocentral adjustments considerably larger. Figure 2 shows 277 (a small random subset of the full data set) representative events with their initial and final locations projected onto the horizontal plane.

Resolution and error

To determine the influence of data variability on the model, a jackknife error analysis was performed (Lees and Crosson, 1989). For the linear inversion this is straight forward and provides an estimate of the variability of the model, over regions that are well sampled, given the variability of the data. For a well-sampled model the jackknife estimates of error have been found to be conservative (Lees, 1989). It should be noted that the jackknife estimates do not always provide reasonable estimates for poorly sampled parts of the model. The slowness estimates for the poorly sampled parts of the model, typically on the perimeters of the dense concentrations of the rays, should be correspondingly adjusted for the associated poor spatial resolution. The jackknife estimates for succeeding iterations of the non-linear inversion were added to the estimates for

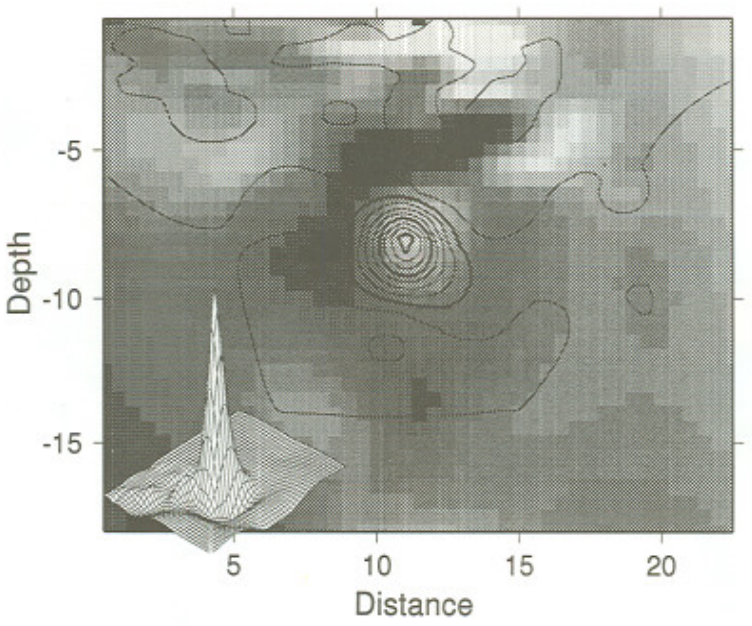

Fig. 3. Vertical cross-section of an example resolution kernel estimated by calculating the impulse response of the system to a spike located at the high-velocity feature at 8 km depth. The greyshades are the slowness perturbations discussed in Figure 5 and the contours are the normalized (to 100%) resolution kernel. The contour interval is 10 and bold contours are highlighted at 10, 50 and 80 unit levels. The inset is a perspective plot of the resolution kernel which emphasizes the high resolution for this region.

the linear inversion. Although there were a few places where the errors were higher, most of the error estimates were in the range of 5% slowness perturbation. For example, in layer 7 (3.5–4.8 km depth) there is an isolated, 1.5 km radius spot southeast of the volcano summit where the error estimates are as high as 10% perturbation. The same place, however, has a slowness perturbation of 22%.

Resolution was estimated by calculating impulse responses for different parts of the model (Humphreys and Clayton, 1988; Lees and Crosson, 1989). The resolution kernels, however, are typically not symmetric, due to heterogeneity of ray coverage. Since the ray coverage is very dense near the center of the model, the resolution below the edifice of Mount St. Helens is nearly one block (slightly over 0.5 km) both in the horizontal and the vertical directions. This estimate includes the effect of ray density and the effect of smoothing by the Laplacian. An example resolution kernel located at 8 km depth is provided in Figure 3. On the edges of the ray coverage and near the bottom of the model the resolution degrades considerably and smearing of the images is inevitable. For this reason I restrict the interpretation only to anomalies located near the center of the model where spatial resolution is reliable.

Results

The results of the inversion are displayed as 12 horizontal layers, partitioned according to the initial reference model (Fig. 4), and an east–west vertical cross-section in Figure 5. The horizontal cross-sections are displayed as perturbations from the reference model where the range of perturbations and actual velocities are indicated for each layer. The cross-sections show the same slowness perturbations sliced along the line *A–A'* indicated in Figure 1, along

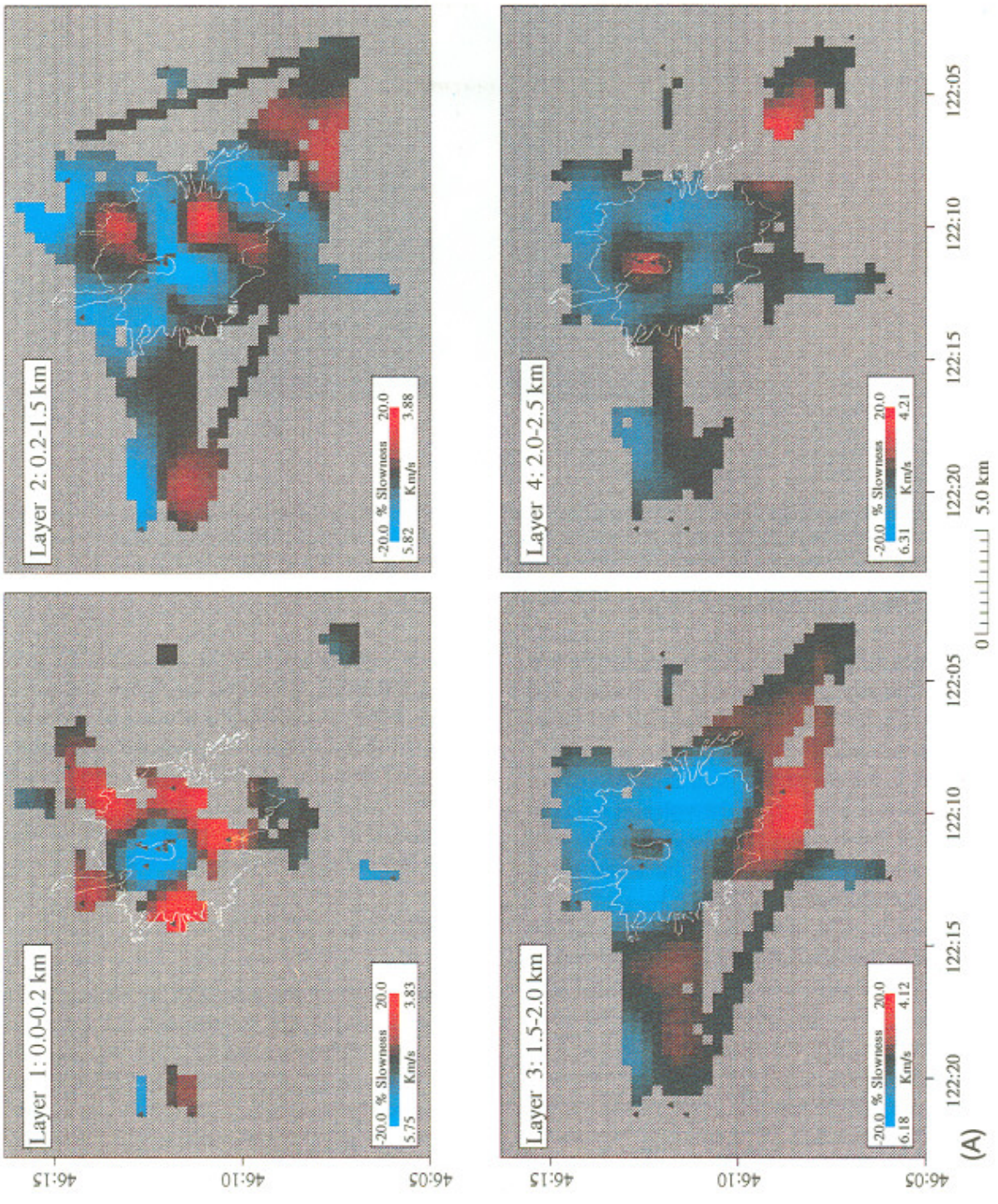
Layer 1: 0.0-0.2 km
-20.0 % Slowness 20.0
5.75 Km/s 3.83
Layer 2: 0.2-1.5 km
-20.0 % Slowness 20.0
5.82 Km/s 3.88
Layer 3: 1.5-2.0 km
-20.0 % Slowness 20.0
6.18 Km/s 4.12
Layer 4: 2.0-2.5 km
-20.0 % Slowness 20.0
6.31 Km/s 4.21
46:15
46:10
46:05
122:20
122:15
122:10
122:05
122:00
0 5.0 km
(A)

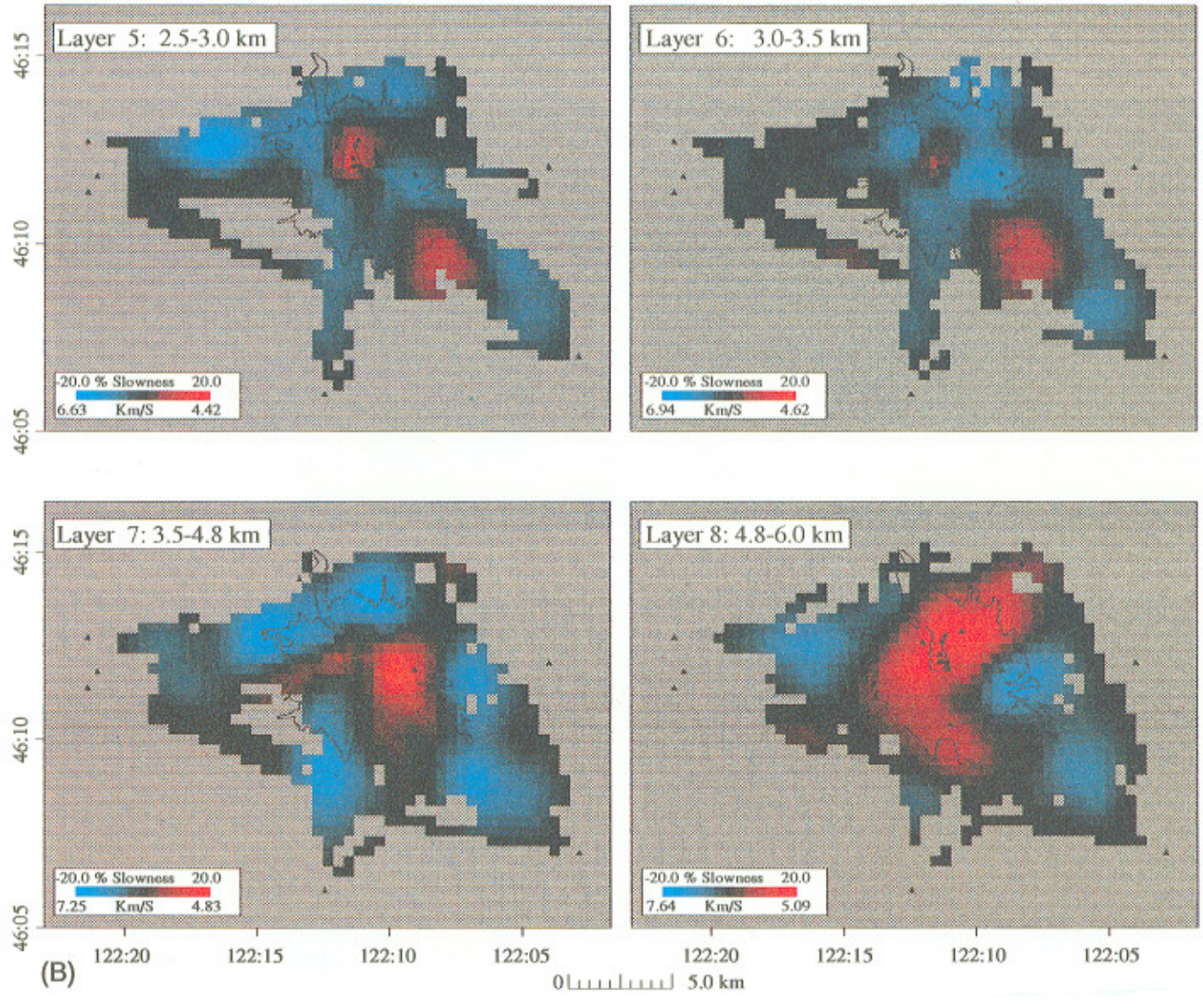
Layer 5: 2.5-3.0 km
-20.0 % Slowness 20.0
6.63 Km/S 4.42
Layer 6: 3.0-3.5 km
-20.0 % Slowness 20.0
6.94 Km/S 4.62
Layer 7: 3.5-4.8 km
-20.0 % Slowness 20.0
7.25 Km/S 4.83
Layer 8: 4.8-6.0 km
-20.0 % Slowness 20.0
7.64 Km/S 5.09
46:15
46:10
46:05
122:20
122:15
122:10
122:05
(B)
0 5.0 km

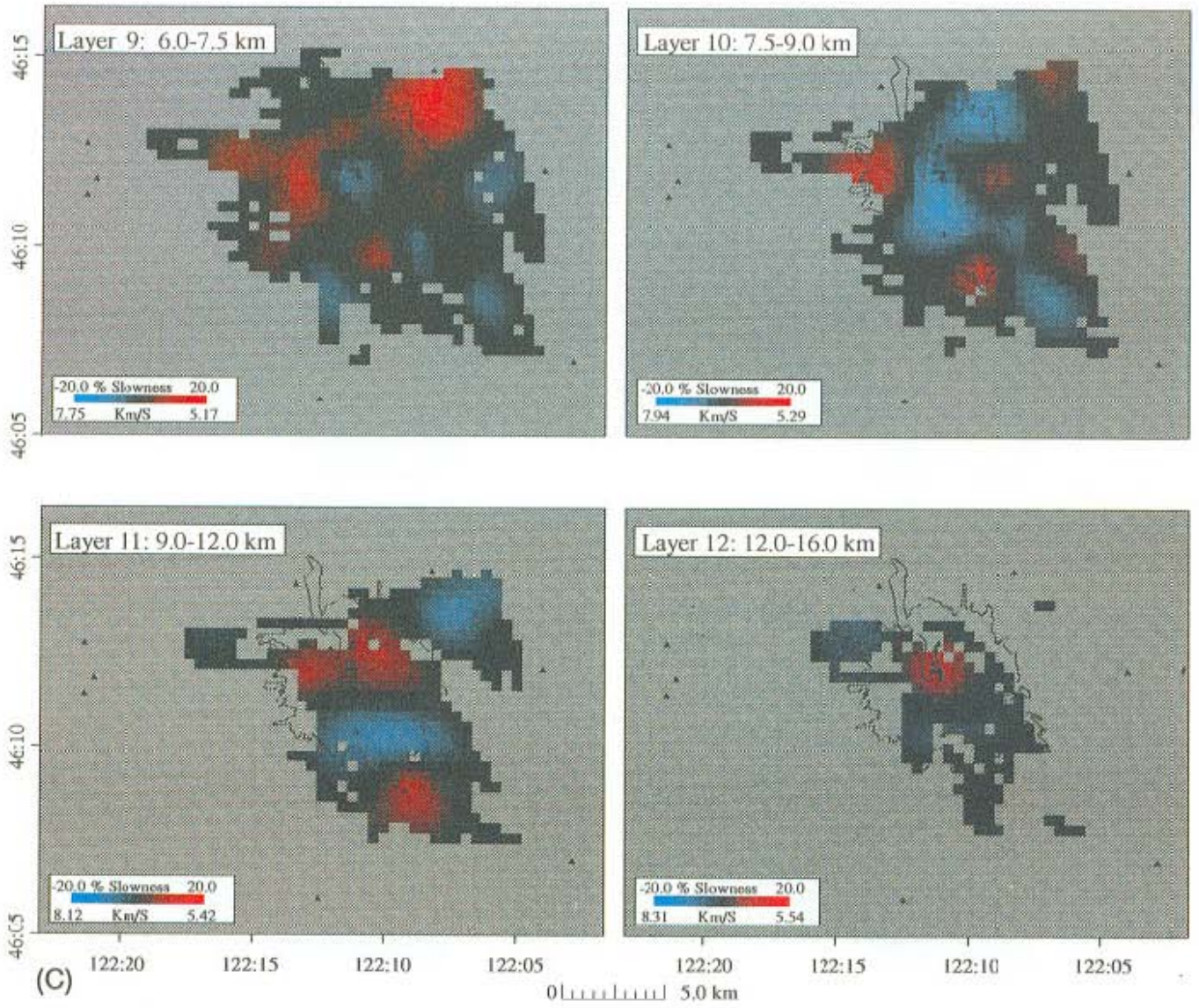

Fig. 4. Slowness perturbations relative to the reference model SH3. Anomalies are represented as percent perturbation from the background. A common ±20% scale is plotted on each layer, where the corresponding velocity values are indicated for each section. Blue colors represent higher-velocity and red represents lower-velocity material

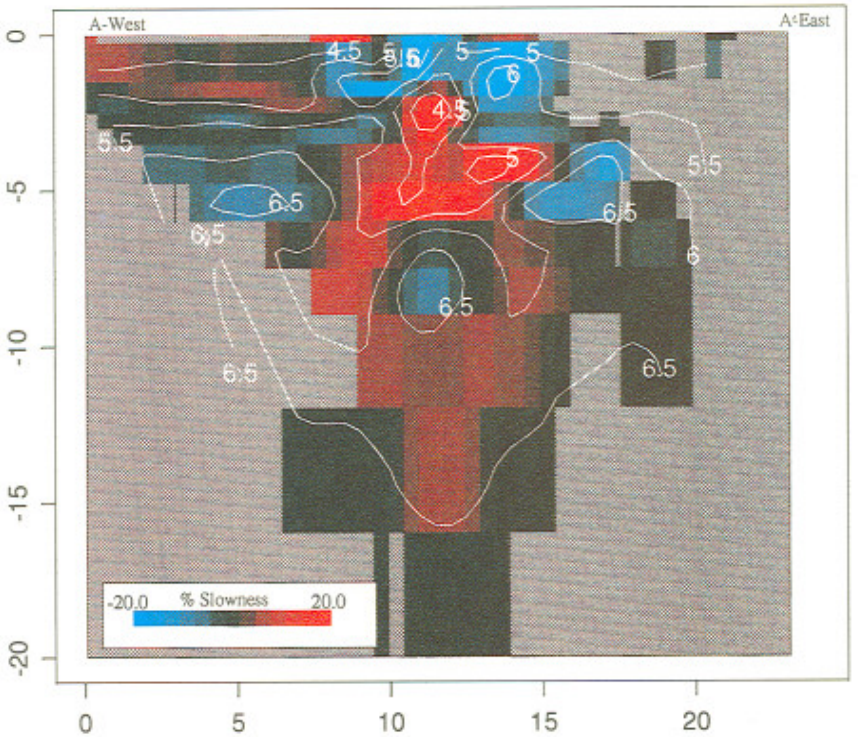

Fig. 5. Cross-section of the slowness perturbations along A–A' (Fig. 1). Contours of the absolute velocities (background plus perturbation) are provided for reference.

with contoured velocities for comparison. Regions of higher velocity are delineated by blue hues and those of lower velocity are red.

Near the surface we observe a high-velocity region extending to about 1.5 km depth below the crater floor. At about 1.5 km depth, directly below the crater, a small low-velocity perturbation, approximately 1–2 km in diameter, is seen surrounded by higher-velocity material. This localized low velocity extends to a depth of 3.5 km depth where it then appears to broaden (4–5 km diameter) and continues to a depth of 7.5 km. Between 6 and 9 km depth a higher-velocity zone is observed below the summit which becomes lower-velocity at 9 to 16 km depth, although the data coverage at this depth is too sparse to make reliable estimates.

Discussion

The high-velocity region below the summit to a depth of 1.5 km has been observed previously (Fehler, 1985) and perhaps represents a zone of solidified magma which has cooled since the most recent eruptions. At 1.5 km depth the apparent high-velocity plug transforms into a low-velocity conduit, or pipe, extending to at least 3.5 km depth. The narrow conduit has been proposed from observations of the spatial distribution of seismicity below the volcano edifice (Shemeta and Weaver, 1986; Endo et al., 1990). In this study I have provided further physical evidence supporting the narrow conduit observation based on the distribution of seismic velocities. At 3.5 km depth the broadening of this anomaly suggests either an accumulation of magma, a shallow magma chamber, or alternatively, a system of conduits and dikes which, because of extensive faulting, or the presence of melt, extends over a 5 km area to a depth of 6 km. At 6 km depth the model departs from previous conceptions of the magma system at Mt. St. Helens. Here a higher-velocity body is observed to a depth of

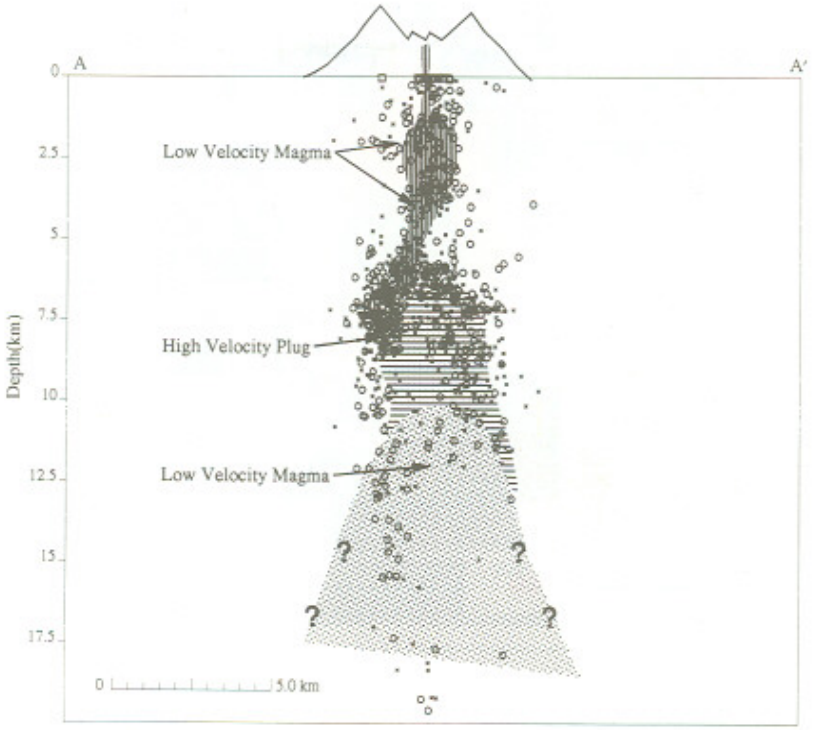

Fig. 6. Schematic interpretation of the model. Low-velocity magma bodies lie above an below a higher-velocity plug where the intense seismicity occurs. Circles represent earthquake locations relative to the SH3 model and ×'s are locations relative to the new three-dimensional model. The overall pattern of seismicity does not appear to have changed significantly.

9 km. Previously accepted models (Scandone and Malone, 1985; Rutherford and Devine, 1988; Lees and Crosson, 1989) suggested a magma body starting at an approximate depth of 7 km. This new model suggests that perhaps there is a high-velocity plug between 6 and 9 km depth at the top of a deeper magma accumulation which is faintly observed starting at 9–16 km. The plug represents a zone of solidified material which sustains stresses associated with the observed high levels of seismicity in this depth range. This places the magma chamber deeper than previous models by 2–3 km. Below the higher-velocity plug, the low velocity of the magma chamber can be seen in this study, although the resolution of the inversion is poor at this depth due to the low density of data coverage.

A schematic model is summarized in Figure 6 where seismicity prior to three-dimensional relocation and the new event locations are both indicated (450 events, selected after the May 18 eruption). The seismicity patterns, used in the previous interpretations of the magma system (Scandone and Malone, 1985; Shemeta and Weaver, 1986) are evident in this figure. The new locations do not significantly alter the previous interpretations, although scattering is evident. For either set of locations the high correlation of seismicity and velocity anomalies strengthens the conclusions of this study.

Conclusion

In this study I have presented a full non-linear, smoothed inversion of the P-wave velocity structure below Mt. St. Helens at spatial resolutions down to 1–2 km. The non-linear inversions, including three-dimensional ray-tracing and hypocenter relocation, did not appear to

differ appreciably from the linear resolutions, at least regarding the interpreted structures. The magma system presented in this study agrees, at least in part, with earlier observations based on seismic, geodetic, gravity, aeromagnetic and geochemical observations. There appears to be a shallow magma reservoir between 3.5 and 6 km depth. A narrow conduit connects this magma accumulation with the surface where higher than normal velocities apparently reflect the solidified edifice of Mt. St. Helens. Below the shallow magma zone there is a high-velocity anomaly (6–9 km depth) which suggests a plug of solidified material where extensive seismicity occurs. Below 9 km depth the data are sparse, and therefore reliable estimates are not available, but a low-velocity anomaly suggests the presence of the magma chamber suggested by seismic, geochemical and geodetic modeling.

Acknowledgements

The author would like to thank Steve Malone, Seth Moran and John VanDecar for many useful discussions. I am grateful for the many helpful comments supplied by Gary Pavlis and an anonymous reviewer. This research was supported under NSF Grant EAR-9096281.

References

Achauer, U., Evans, J.R. and Stauber, D.A., 1988. High-resolution seismic tomography of compressional wave velocity structure at Newberry Volcano, Oregon Cascade range. J. Geophys. Res., 93: 10,135–10,147.

Aki, K., Christoffersson, A. and Husebye, E.S., 1977. Determination of the three-dimensional seismic structure of the lithosphere. J. Geophys. Res., 82: 277–296.

Aster, R.C. and Meyer, R.P., 1988. Three-dimensional velocity structure and hypocenter distribution in the Campi Flegrei caldera, Italy. Tectonophysics, 149: 195–218.

Barker, S.E. and Malone, S.D., 1991. Magmatic system geometry at Mt. St. Helens modeled from the stress field associated with posteruptive earthquakes. J. Geophys. Res., 96: 11,883–11,894.

Endo, E.T., Dzurisin, D. and Swanson, D.A., 1990. Geophysical and observational constraints for the ascent rates of dacitic magma at Mount St. Helens. In: M.P. Ryan (Editor), Magma Transport and Storage. Wiley, Chichester, pp. 317–334.

Evans, J.R. and Zucca, J.J., 1988. Active high-resolution seismic tomography of compressional wave velocity and attenuation structure at Medicine Lake volcano, northern California Cascade Range. J. Geophys. Res., 93: 15,016–15,036.

Fehler, M., 1985. Locations and spectral properties of earthquakes accompanying an eruption of Mount St. Helens. J. Geophys. Res., 90: 12,729–12,740.

Finn, C. and Williams, D.L., 1987. An aeromagnetic study of Mount St. Helens. J. Geophys. Res., 92: 10,194–10,206.

Humphreys, E. and Clayton, R.W., 1988. Adaptation of back projection tomography to seismic travel time problems. J. Geophys. Res., 93: 1073–1085.

Iyer, H.M., Evans, J.R., Dawson, P.B., Stauber, D.A. and Achauer, U., 1990. Differences in magma storage in different volcanic environments as revealed by seismic tomography: silicic volcanic centers and subduction-related volcanoes. In: M.P. Ryan (Editor), Magma Transport and Storage. Wiley, Chichester, pp. 293–316.

Kissling, E., 1988. Geotomography with local earthquake data. Rev. Geophys., 26: 659–698.

Lees, J.M., 1989. Seismic Tomography in Western Washington. Ph.D. Thesis, University of Washington.

Lees, J.M. and Crosson, R.S., 1989. Tomographic inversion for three-dimensional velocity structure at Mount St. Helens using earthquake data. J. Geophys. Res., 94: 5716–5728.

Malone, S.D. and Pavlis, G.L., 1983. Velocity structure and relocation of earthquakes at Mount St. Helens. Eos Trans. AGU, 64: 895.

Moser, T.J., 1991. Shortest path calculation of seismic rays. Geophysics, 56: 59–67.

Pavlis, G.L. and Booker, J.R., 1980. The mixed discrete–continuous inverse problem: application to the simultaneous determination of earthquake hypocenters and velocity structure. J. Geophys. Res., 85: 4801–4810.

Pavlis, G.L. and Booker, J.R., 1983. Progressive multiple event location (PMEL). Bull. Seismol. Soc. Am., 73: 1753–1777.

Rutherford, M.J. and Devine, J.D., 1988. The May 18, 1980, eruption of Mount St. Helens, 3. Stability and chemistry of amphibole in the magma chamber. J. Geophys. Res., 93: 11,949–11,959.

Rutherford, M.J., Sigurdsson, H., Carey, S. and Davis, A., 1985. The May 18, 1980, eruption of Mount St. Helens, 1. Melt composition and experimental phase equilibria. J. Geophys. Res., 90: 2929–2947.

Scandone, R. and Malone, S.D., 1985. Magma supply, magma discharge and readjustment of the feeding system of Mount St. Helens during 1980. J. Volcanol. Geotherm. Res., 23: 238–262.

Shaw, P.R. and Orcutt, J.A., 1985. Waveform inversion of seismic refraction data and applications to young

Pacific crust. Geophys. J. R. Astron. Soc., 82: 375–414.
Shemeta, J.E. and Weaver, C.S., 1986. Seismicity accompanying the May 18, 1980 eruption of Mount St. Helens, Washington. In: S.A.C. Keller (Editor), Mount St. Helens: Five Years Later. Eastern Washington University Press, Chency, WA, pp. 44–58.
Thurber, C.H., 1983. Earthquake locations and three-dimensional crustal structure in the Coyote Lake area, central California. J. Geophys. Res., 88: 8226–8236.
Thurber, C.H., 1984. Seismic detection of the summit magma complex of Kilauea volcano, Hawaii. Science, 233: 165–167.
Um, J. and Thurber, C., 1987. A fast algorithm for two-point seismic ray tracing. Bull. Seismol. Soc. Am., 77: 972–986.
VanDecar, J.C., 1991. Upper-Mantle Structure of the Cascadia Subduction Zone from Non-Linear Teleseismic Travel-Time Inversion. Ph.D. Thesis, University of Washington, Seattle, WA.
Weaver, C.S. and Smith, S.W., 1983. Regional tectonic and earthquake hazard implications of a crustal fault zone in southwestern Washington. J. Geophys. Res., 88: 10,371–10,383.
Weaver, C.S., Grant, W.C. and Shemeta, J.E., 1987. Local crustal extension at Mount St. Helens, Washington. J. Geophys. Res., 92: 10,170–10,178.
Williams, D.L., Abrams, G., Finn, C., Dzurisin, D., Johnson, D.J. and Denlinger, R., 1987. Evidence from gravity data for an intrusive complex beneath Mount St. Helens. J. Geophys. Res., 92: 10,207–10,222.